

An ambidextrous polyphenol glycosyltransferase *PaGT2* from *Phytolacca americana*

rakesh maharjan, Yohta Fukuda, Naomichi Shimomura, Taisuke Nakayama, Yuta Okimoto,
Koki Kawakami, Toru Nakayama, Hiroki Hamada, Tsuyoshi Inoue, and Shin-ichi Ozaki

Biochemistry, **Just Accepted Manuscript** • DOI: 10.1021/acs.biochem.0c00224 • Publication Date (Web): 11 Jun 2020

Downloaded from pubs.acs.org on June 18, 2020

Just Accepted

“Just Accepted” manuscripts have been peer-reviewed and accepted for publication. They are posted online prior to technical editing, formatting for publication and author proofing. The American Chemical Society provides “Just Accepted” as a service to the research community to expedite the dissemination of scientific material as soon as possible after acceptance. “Just Accepted” manuscripts appear in full in PDF format accompanied by an HTML abstract. “Just Accepted” manuscripts have been fully peer reviewed, but should not be considered the official version of record. They are citable by the Digital Object Identifier (DOI®). “Just Accepted” is an optional service offered to authors. Therefore, the “Just Accepted” Web site may not include all articles that will be published in the journal. After a manuscript is technically edited and formatted, it will be removed from the “Just Accepted” Web site and published as an ASAP article. Note that technical editing may introduce minor changes to the manuscript text and/or graphics which could affect content, and all legal disclaimers and ethical guidelines that apply to the journal pertain. ACS cannot be held responsible for errors or consequences arising from the use of information contained in these “Just Accepted” manuscripts.

An ambidextrous polyphenol glycosyltransferase *PaGT2* from *Phytolacca americana*

Rakesh Maharjan,^{†,‡} Yohta Fukuda,^{†,‡} Naomichi Shimomura,[‡] Taisuke Nakayama,[§] Yuta Okimoto,[‡] Koki Kawakami,^{||} Toru Nakayama,[#] Hiroki Hamada,^{*} Tsuyoshi Inoue,^{*,†,‡} Shin-ichi Ozaki^{*,‡}

[†]Department of Applied Chemistry, Graduate School of Engineering, Osaka University, Suita City, Osaka 565-0871, Japan

[‡]Graduate School of Pharmaceutical Science, Osaka University, Suita City, Osaka 565-0871, Japan

[‡]Department of Biological Chemistry, Graduate School of Science and Technology for Innovations, Yamaguchi University, Yamaguchi 753-8515, Japan

[§]National Institute of Biomedical Innovation, Health and Nutrition, Saito-Asagi, Ibaraki City, Osaka 567-0085, Japan

[#]Department of Biomolecular Engineering, Graduate School of Engineering, Tohoku University, Sendai, Miyagi 980-8579, Japan

^{||}Department of Life Science, Faculty of Science, Okayama University of Science, Okayama 700-0005, Japan

ABSTRACT: The glycosylation of small hydrophobic compounds is catalyzed by uridine diphosphate glycosyltransferases (UGTs). Since glycosylation is an invaluable tool for improving stability and water solubility of hydrophobic compounds, UGTs have gained attention for their application in food, cosmetics, and pharmaceutical industries. However, the ability of UGTs to accept and glycosylate a wide range of substrates is not clearly understood due to the existence of a large number of UGTs. *PaGT2*, a UGT from *Phytolacca americana* can regioselectively glycosylate piceatannol but has low activity towards other stilbenoids. To elucidate the substrate specificity and catalytic mechanism, we determined the crystal structures of *PaGT2* with and without substrates and performed molecular docking studies. The structures have revealed key residues involved in substrate recognition and suggest the presence of a non-conserved catalytic residue (His81) in addition to the highly conserved catalytic histidine in UGTs (His18). The role of the identified residues in substrate recognition and catalysis is elucidated with the mutational assay. Additionally, the structure-guided mutation of Cys142 to other residues, Ala, Phe, and Gln, allows *PaGT2* to glycosylate resveratrol with high regioselectivity, which is negligibly glycosylated by the wildtype enzyme. These results provide a basis for tailoring an efficient glycosyltransferase.

INTRODUCTION

Glycosyltransferases (GTs) catalyze the transfer of a sugar moiety from activated sugar donor to acceptors.¹ GTs play a major role in cellular localization, storage, or metabolism of metabolites and xenobiotic compounds, thereby maintaining the cellular homeostasis.² Natural products such as polyphenols are usually glycosylated.^{3–5} Glycosylation improves water solubility and chemical stability of polyphenols, preserving their bioactivity.⁶ Polyphenols and their glycosides are known to have several health benefits such as antioxidant, anti-aging, anti-estrogenic, anticancer, anti-inflammatory, and cardio-protective effects.^{7–10} Though glycosylation of polyphenols can be achieved by chemical synthesis, these methods are limited by poor regioselectivity and involve tedious steps of protection and deprotection of functional groups.¹¹ Contrary to this, enzyme-mediated glycosylation is more efficient and highly regioselective.¹²

Glycosylation of small hydrophobic compounds in plants is catalyzed mainly by uridine diphosphate glycosyltransferases (UGTs), classified as the GT1 family in the carbohydrate-active enzyme (CAZy) database.¹³ Recently, several plant and bacterial UGTs are characterized for their ability to glycosylate different polyphenols.^{14–19} The determination of crystal structures of UGTs such as VvGT1²⁰ from *Vitis vinifera*, UGT85H2²¹, UGT71G1²² from *Medicago truncatula*, UGT78K6²³ from *Clitoria ternatae*, OleD and

OleI²⁴ from *Streptomyces antibioticus*, and others have provided a basis for the understanding of the glycosylation mechanism in plant UGTs. Besides, site-directed mutagenesis and directed evolution of UGTs have been studied for enhancing the enzyme's activity and/or changing the regioselectivity of glycosylated products.^{25–29} Plant UGTs are characterized by the presence of a highly conserved plant secondary product glycosyltransferase (PSPG) motif that is involved in the recognition of the UDP-sugar donor.³⁰ Although the residues involved in recognition of sugar-acceptor in UGTs are less conserved, a highly conserved histidine-aspartate (His-Asp) pair has been identified to catalyze the glycosylation.^{31–34} The catalytic pair is involved in the removal of a proton from the glycosylation site to generate a nucleophile that attacks the C1 carbon atom of the sugar moiety.³⁴ However, UGTs with non-conserved catalytic residue^{35,36} or without catalytic pair³² are known to catalyze glycosylation. This necessitates the exploration of more UGTs for improving our understanding of enzymatic glycosylation.

Glucosides of compounds such as kaempferol, quercetin, and triterpene saponins have been extracted from various parts of a toxic plant *Phytolacca americana*.³⁷ The cell suspension of *P. americana* is also able to glucosylate exogenous compounds such as resveratrol, perillyl alcohol, and, 2,2,5,7,8-pentamethyl-6-chromanol.³⁸ *PaGT2*, a glycosyltransferase from *P. americana* regioselectively glycosylates piceatannol (3, 5, 3', 4'-tetrahydroxystilbene), a stilbenoid polyphenol, while it has negligible activity with resveratrol

(3, 5, 4'-tetrahydroxystilbene) which lacks a hydroxyl group. This bias in the substrate specificity of *PaGT2* could not be explained as UGT structures with stilbenoids are not available. Herein, we determined the crystal structures of *PaGT2* with and without stilbenoid substrates. Together with molecular docking, we identified the key residues for substrate recognition and found that *PaGT2* catalyzes glycosylation through two individual catalytic residues. Additionally, the structure-guided mutagenesis allowed *PaGT2* to glycosylate resveratrol with high regioselectivity, which was negligibly glycosylated by the wildtype enzyme.

MATERIALS AND METHODS

Expression and purification of *PaGT2*. *PaGT2* cDNA and pCold vector were amplified by polymerase chain reaction (PCR) using following primers: pCold forward 5'-TAGGTAATCTCTGCTTAAAAGCACAG-3', pCold reverse 5'-ACCCTGGAAATAAAGATTCTCC-3', *PaGT2* forward 5'-CTTTATTTCCAGGGTATGGAAATGGAAGCACCCTC-3', and *PaGT2* reverse 5'-AGCAGAGATTACCTAGCTTTTGCATTGGCTCCATTAG-3'. Amplified *PaGT2* cDNA was cloned into the pCold vector using the Infusion kit (Takara Bio USA, Inc.) following the manufacturer's protocol. The construct contained N-terminal 6x histidine tag followed by a TEV protease recognition site. A single colony of *E. coli* BL21 Star (DE3), transformed with pCold *PaGT2*, was inoculated into 2 ml LB medium supplemented with 100 µg/ml ampicillin and grown at 37 °C for about 8 hours as a starter culture. 200 µl of the starter culture was introduced into a 200 ml LB medium with the same concentration of antibiotics and grown overnight at 37 °C. This culture was used to inoculate 1 L culture in the same medium in the next morning and the cells were continued to grow at 37 °C. When the OD₆₀₀ was ~0.4, the temperature was decreased to 15 °C. Expression was induced with isopropyl-β-D-thiogalactopyranoside (IPTG) at 15 °C and OD₆₀₀ ~0.6-0.8. After 24 hours, cells were harvested by centrifugation at 9000 × g for 10 min at 4 °C. Harvested cells were frozen with liquid nitrogen and stored at -80 °C until its use.

The cell pellet was re-suspended in buffer A (20 mM Tris-HCl pH 8.5, 100 mM NaCl, 5 mM DTT) including 1 tablet of a protease inhibitor cocktail (Roche). Cells were lysed by sonication on ice with the following pulse sequence: 15-sec burst, 15-sec rest for a total burst time of 10 min at a power output of 80. Lysed cells were subjected to centrifugation at 20,000 ×g for 30 min at 4 °C. The obtained supernatant was filtered using a 0.45 µm membrane syringe filter. The filtered supernatant was loaded on to a Ni-NTA column (HisTrap HP 5 ml) equilibrated with buffer A. The column was washed with 10 column volume (CV) of buffer A. bound protein was eluted with a 0-50% gradient of buffer A supplemented with 300 mM imidazole. Fractions containing *PaGT2* were pooled, mixed with TEV protease, and dialyzed overnight against buffer A to remove the histidine tag. The dialyzed sample was diluted 10 times using 20 mM Tris-HCl pH 8.5 and loaded on to a HiTrap Q (5 ml) column equilibrated with 20 mM Tris-HCl pH 8.5. *PaGT2* was eluted with a linear gradient ranging from 0 to 1 M NaCl in 20 mM Tris-HCl pH 8.5. Fractions containing *PaGT2* were pooled, concentrated using a 30 kDa MWCO Vivaspin tube (Sartorius), and loaded on to a Hiload 16/60 Superdex 200 pg size exclusion chromatography (SEC) column equilibrated with an SEC buffer (20 mM Tris-HCl pH 8.0, 100 mM NaCl, 5 mM DTT). Fractions containing *PaGT2* were pooled, concentrated, and stored at -80 °C.

Site-directed mutagenesis. Site-directed mutagenesis was performed using the whole plasmid pCold-*PaGT2* and specific oligonucleotide primers listed in Table S1. Briefly, the whole plasmid was linearized with mutagenesis primers by PCR. Amplified PCR products were treated with DpnI (New England Biolabs) and purified using NucleoSpin® Gel and PCR Clean-up (Macherey-Nagel), following the manufacturer's protocol. The purified PCR product was ligated using T4-polynucleotide kinase (Toyobo co.) and ligation high ver. 2.0 (Toyobo co.), and transformed into *E. coli* DH5a. The desired mutation of *PaGT2* was confirmed by DNA sequencing.

Enzyme assay. Wildtype *PaGT2* and all mutants for enzyme assay were expressed and purified as mentioned above. The glycosylation reactions were performed at 37°C in a 200 µl total reaction volume. The structure of the substrates used and the HPLC profile of the reaction mixture after the glycosylation reaction is shown in Figure 1. The reaction solution containing 50 mM potassium phosphate buffer (pH 7.4), 50 µM acceptor substrates, 100 µM UDP-Glucose, and 5 µM enzyme was incubated at 37°C for 10 minutes. The reaction was stopped by adding 1.5% trifluoroacetic acid, centrifuged at 12,000 rpm for 1 minute, and filtered using a discmic-13HP filter. HPLC analysis of the reaction mixtures was performed on an Impact US-C18 (2.0 × 150 mm) reverse-phase column at a flow rate of 0.2 mL/min. Piceatannol and resveratrol glycosylation mixtures were analyzed by isocratic elution, starting with 15% acetonitrile and 85% water for 20 minutes followed by 100% acetonitrile for 10 minutes. Rhapontigenin glycosylation mixtures were also analyzed by isocratic elution, starting with 50% acetonitrile and 50% water for 30 minutes followed by 100% acetonitrile for 10 minutes. Kaempferol glycosylation products were eluted by a linear gradient of acetonitrile starting from 10% acetonitrile and 90% water to 30% acetonitrile and 70% water in 20 minutes followed by 100% acetonitrile for 10 minutes. Pterostilbene glycosylation products were also eluted using a linear gradient of 50% acetonitrile and 50% water to 100% acetonitrile in 30 minutes followed by 100% acetonitrile for 10 minutes. The glucoside products were identified by comparison of the HPLC chromatograms of the reaction mixtures with the chromatograms of standard samples of respective compounds.³⁹ However, the obtained kaempferol product glycosylated by *PaGT2*, kaempferol 3-*O*-β-glucoside, and kaempferol 4'-*O*-β-glucoside were eluted at the nearly same time (Figure S1A). Thus, the regioselectivity of kaempferol glucoside products by wildtype *PaGT2* was determined by a nuclear magnetic resonance (NMR) method (Figure S1B). ¹H NMR spectral data were recorded using a JEOL 400 MHz NMR spectrometer in DMSO-*d*₆ and compared with known chemical shift values of authentic kaempferol 3-*O*-β-glucoside or kaempferol 4'-*O*-β-glucoside. The chemical shift and coupling constants are expressed in δ (ppm) and Hz, respectively. The anomeric proton signal of the kaempferol product appeared at δ 5.20 (1H, d, J=7.2 Hz). The observed chemical shift value is similar to δ 5.25 (1H, d, J=7.6 Hz) obtained with standard kaempferol 3-*O*-β-glucoside and different from δ 5.03 (1H, d, J=7.0 Hz) reported for kaempferol 4'-*O*-β-glucoside.⁴⁰ To quantitate glucoside products in the reaction mixture, standard curves were generated. For enzyme kinetic studies, acceptor concentrations were varied (25-150 µM). To determine the *K*_m values of less than 30 µM in Table 1, we varied the acceptor concentration from 7.5-150 µM. The final concentration of piceatannol and kaempferol was determined based on extinction coefficients reported previously (piceatannol 26,350 M⁻¹cm⁻¹ at 304 nm in ethanol⁴¹, kaempferol 21,242 M⁻¹cm⁻¹ at 365 nm in methanol⁴²). The hyperbolic dependence of glucoside production rates on acceptor concentrations was

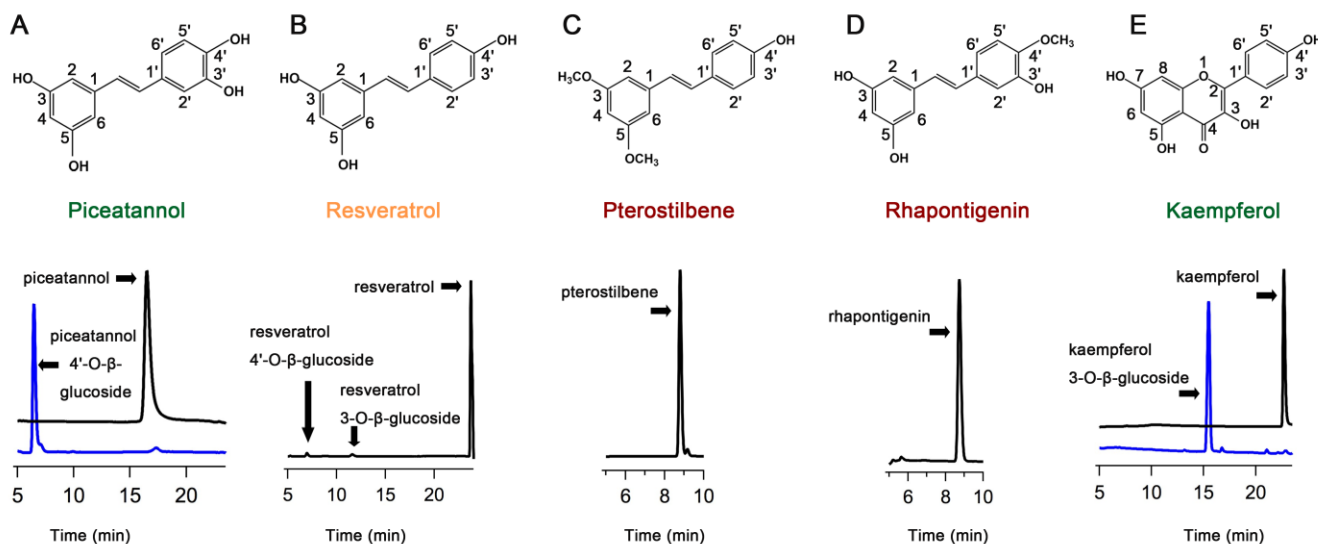


Figure 1: Structure of aglycones utilized for glycosylation assay and HPLC analysis chromatogram. Aglycones for glycosylation A) Piceatannol, B) Resveratrol, C) Pterostilbene, D) Rhapontigenin, and E) Kaempferol and the HPLC chromatograms (below) after the glycosylation reaction by *PaGT2* utilizing donor UDP-glucose. For piceatannol and kaempferol, black and blue lines indicates the elution profile of standard compound and the products of glycosylation by *PaGT2*, respectively. For resveratrol, pterostilbene, and rhapontigenin, HPLC chromatograms of the reaction mixture is shown. The names of aglycones are colored green, orange, and red indicating good, poor, and not substrates for *PaGT2*, respectively.

fitted using the Michaelis–Menten equation to determine the k_{cat} and K_m values.

Protein crystallization. Crystallization screening of *PaGT2* with and without resveratrol and UDP-2FGlc were performed by the sitting drop vapor diffusion method from 1:1 mixture of 100 nL protein stock (15 mg/ml in 20 mM Tris-HCl pH 8.0, 100 mM NaCl, 5 mM DTT) and 100 nL well solution. Apo *PaGT2* was crystallized using well solution containing 0.1 M magnesium formate, 0.1 M MOPS pH 7.0, and 17% w/v PEG 3350 at 20 °C. Optimal crystals for diffraction were achieved by micro-seeding and hanging drop vapor diffusion from 1:1 mixture of protein (1 μ l) and reservoir solution (1 μ l). Crystals were harvested in the same reservoir solution supplemented with 15% ethylene glycol and flash cooled in liquid nitrogen.

Complexes of *PaGT2* with UDP-2FGlc and resveratrol/pterostilbene were obtained by co-crystallization in the presence of 5 mM UDP-2FGlc and 2 mM resveratrol/pterostilbene in ethanol. Crystals were grown by the hanging-drop vapor diffusion method in 1:1 mixture of protein solution and the reservoir solution containing 0.11 M potassium citrate, 0.06 M lithium citrate, 0.11 M sodium phosphate, and 23–25% w/v PEG 6000. Crystals were harvested in the same reservoir solution supplemented with 15% xylitol and flash cooled in liquid nitrogen.

Data collection and crystal structure determination. Diffraction data were collected on a beamline BL44XU at SPring-8 with an MX300HE CCD detector (Rayonix, LLC) and an EIGER X 16M detector (Dectris). The data for apo-*PaGT2* was collected to 2.30 Å. The data of *PaGT2* complexed with UDP-2FGlc acceptors resveratrol or piceatannol were collected to 2.60 Å and 2.65 Å, respectively. X-ray diffraction data were indexed and scaled using HKL2000⁴³ or XDS.⁴⁴ The structure of apo *PaGT2* was solved by molecular replacement using *Arabidopsis thaliana* UGT72B1

(PDB: 2VCH) as a search model using Molrep⁴⁵ in CCP4.⁴⁶ The structures of *PaGT2* complexes were solved using the solved apo-*PaGT2* structure as a search model. Model building and refinement were performed using COOT⁴⁷ and refmac5.⁴⁸ Figures were prepared using PyMol⁴⁹ and LigPlot+.⁵⁰

Molecular Docking. Molecular docking of piceatannol and kaempferol were performed using an automatic docking program PyRx Virtual Screening tool.⁵¹ The crystal structure of *PaGT2* in complex with UDP-2FGlc and resveratrol was used as a reference after removing the ligands. Ligands for docking- piceatannol, and kaempferol were obtained from the COOT library and saved in the .pdb format. Both protein and ligands were opened in the PyRx program. *PaGT2* chosen as the macromolecule and piceatannol/kaempferol as ligand were automatically converted to the .pdbqt format. The center of the grid box was set to (X= 25.09, Y= 48.81, and Z=72.93) and the dimension of the grid box was set to (6.64×15.65×5.26) together with exhaustiveness 8. Docking was performed with AutoDock Vina⁵² in PyRx. Molecular docking of resveratrol and pterostilbene were also performed using the same grid box parameters to confirm the accuracy of molecular docking. To evaluate the binding affinity of acceptors in the active-site in His18/81Ala double mutant, a model of *PaGT2* with His18/81Ala mutation was prepared using COOT. Molecular docking of all four acceptors was performed also performed with the *PaGT2* His18/81Ala mutant model. PyMol was used for visualization of the results and preparation of figures. Figures of molecular docking show the binding modes of acceptors with high possibilities.

RESULTS AND DISCUSSION

Glucosylation of stilbenoids by *PaGT2*. Stilbenoid glucosylation ability of *PaGT2* was screened against a panel of stilbenoids using

Table 1. Kinetic parameters of *PaGT2* and mutants

Enzyme (<i>PaGT2</i>)	Acceptor	K_m (μM)	k_{cat} (s^{-1})	k_{cat}/K_m ($\text{M}^{-1} \text{s}^{-1}$)
WT	Piceatannol	31 \pm 1*	1.49 $\times 10^{-2}$ \pm 1.41 $\times 10^{-3}$	480.64 \pm 45
H18A		17 \pm 3	3.70 $\times 10^{-3}$ \pm 6.08 $\times 10^{-4}$	217.64 \pm 28
H81A		52 \pm 3	8.66 $\times 10^{-3}$ \pm 1.83 $\times 10^{-3}$	166.66 \pm 36
E82A		40 \pm 3	4.33 $\times 10^{-3}$ \pm 1.16 $\times 10^{-3}$	108.33 \pm 30
C142A		49 \pm 2	2.16 $\times 10^{-2}$ \pm 1.66 $\times 10^{-3}$	442.17 \pm 38
H18A/H81A		N.D.	N.D.	N.D.
WT	Kaempferol [†]	33 \pm 7	3.66 $\times 10^{-3}$ \pm 3.33 $\times 10^{-4}$	111.11 \pm 25
H18A		25 \pm 2	3.40 $\times 10^{-3}$ \pm 2.11 $\times 10^{-4}$	137.24 \pm 8
H81A		64 \pm 5	6.16 $\times 10^{-3}$ \pm 1.66 $\times 10^{-3}$	96.35 \pm 27
E82A		40 \pm 2	6.17 $\times 10^{-3}$ \pm 1.36 $\times 10^{-4}$	157.99 \pm 7
C142A		41 \pm 2	5.16 $\times 10^{-3}$ \pm 1.17 $\times 10^{-4}$	127.65 \pm 4
H18A/H81A		N.D.	N.D.	N.D.
WT	Resveratrol	N.D.	N.D.	N.D.
WT	Pterostilbene	N.D.	N.D.	N.D.
WT	Rhapontigenin	N.D.	N.D.	N.D.

* Data are presented by means \pm SEM (standard error of the mean, n = 3).

[†] Kinetic parameters for kaempferol determined for overall glucoside products. The H18A, E82A, and C142A mutants produced a mixture of glucosides including kaempferol 3-*O*- β -glucoside.

N.D.: no detectable activity

uridine diphosphate glucose (UDP-Glc) as the glucose donor (Figure 1, Table 1). The products were determined by comparing the HPLC chromatograms with that of the standard samples.³⁹ Among the stilbenoids, *PaGT2* was highly specific towards piceatannol and exclusively formed piceatannol 4'-*O*- β -glucoside. Glycosylation of resveratrol produced a trace amount of both resveratrol 3-*O*- β -glucoside and resveratrol 4'-*O*- β -glucoside. Although the structures of pterostilbene and rhapontigenin are comparable to resveratrol and piceatannol, respectively, no peaks for their glycosylated products were observed. A previous study shows that *PaGT2* actively glycosylates different flavonoids and iso-flavonoids.^{15,38} To elucidate the difference between the mechanism of stilbenoid and flavonoid glycosylation, we performed glycosylation of kaempferol as a representative flavonoid. *PaGT2* regioselectively produced only one kaempferol glucoside (Figure 1, Table 1). Comparison of the HPLC chromatogram with those of standard kaempferol glucosides indicated that *PaGT2* synthesized kaempferol 3-*O*- β -glucoside or kaempferol 4'-*O*- β -glucoside. The product was further analyzed by a nuclear magnetic resonance (NMR) technique and determined to be kaempferol 3-*O*- β -glucoside (Figure S1).

The K_m values for piceatannol and kaempferol were determined to be 29 μM and 33 μM , respectively. A comparison of the catalytic efficiency (k_{cat}/K_m) showed that *PaGT2* could glycosylate piceatannol \sim 4.5 times more efficiently than kaempferol at identical reaction conditions. Interestingly, both piceatannol and kaempferol have four possible glycosylation sites. However, *PaGT2* regioselectively glycosylated only the 4' position in piceatannol and 3 positions in kaempferol. To elucidate the molecular basis for this intriguing reactivity of *PaGT2*, we performed structural analysis as follows.

Crystal structure of *PaGT2*. The crystal structure of apo-*PaGT2* was solved by molecular replacement using the structure of *Ara-bidopsis thaliana* UGT72B1 (PDB: 2VCH)³¹ and refined to 2.30 Å resolution (Figure 2A, Table S2). The asymmetric unit (a.u.) contains two *PaGT2* molecules that are highly similar to each other with overall root mean square deviation (rmsd) of 0.46 Å for overlap of 450 C α atoms. The structure of *PaGT2* belongs to GT-B fold made up of two Rossmann ($\beta/a/\beta$) domains³⁴ and a kinked C-terminal helix that crossed over to the N-terminal domain⁵³, which is a characteristic feature of UGTs with GT-B fold structures. The flexible linker connecting N-terminal (Ala5-Ser243) and C-terminal (Ser252-Gln466) domains is disordered in the structure. Although *PaGT2* is a monomer in solution (Figure S2), the two *PaGT2* molecules present in the a.u. formed a dimer through the insertion of a long loop from the opposite molecule into the substrate-binding pocket.

The structural homology search using the DALI server⁵⁴ shows that the amino acid sequence and the structure of *PaGT2* are highly similar to an indoxyl glucosyltransferase *PtUGT1*⁵⁵ (PDB: 5NLM; sequence identity \sim 56%; rmsd \sim 1.9 Å) and a bifunctional *N*- and *O*-glucosyltransferase *AtUGT72B1*³¹ (PDB: 2VCH; sequence identity \sim 59%; rmsd \sim 2.3 Å). These UGTs are involved in glucosylation of non-polyphenol molecules such as indoxyl sulfate and trichlorophenol, respectively. *PaGT2* also shares high structural homology with other plant UGTs whose structures have been solved. *PaGT2* has sequence similarity of \sim 40% with a C-glycosyltransferase *TcCGT*⁵⁶ (PDB: 6JTD; rmsd \sim 3.0 Å), \sim 31% with a multifunctional triterpene/flavonoid UGT71G1⁵⁷ (PDB: 2ACV; rmsd \sim 2.5 Å), \sim 32% with a multifunctional (iso)flavonoid glycosyltransferase UGT85H2²¹ (PDB: 2PQ6; rmsd \sim 2.4 Å), and \sim 24% with a flavonoid 3-*O*-glucosyltransferase *VvGT1*²⁰ (PDB: 2C1Z; rmsd \sim 3.0 Å).

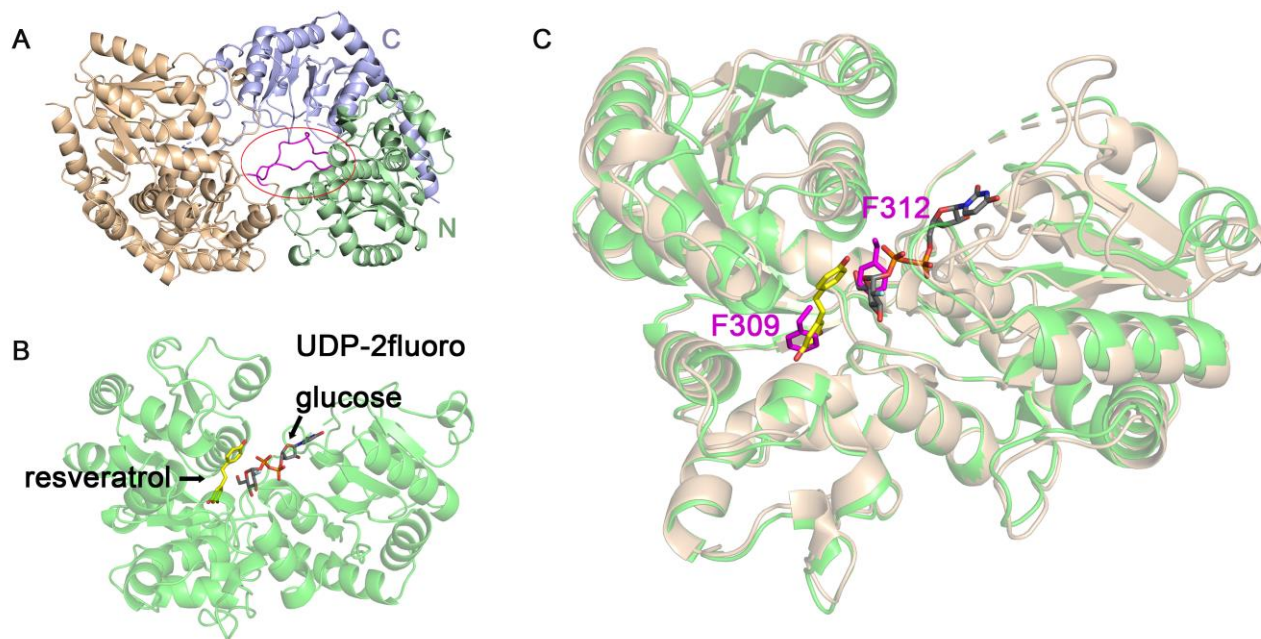


Figure 2: Structures of *PaGT2*. (A) Molecules of apo-*PaGT2* in the a.u. of the crystal structure. The N-terminal domain (light-green), C-terminal domain (light-blue), and the loop inserted into the active-site (magenta, highlighted by a red oval) is indicated in one of the molecules of the a.u. The other molecule in the a.u. is illustrated by light orange. (B) Resveratrol and UDP-2FGlc bound to one of the molecules of *PaGT2* in the a.u. (C) Substrate induced domain movements are seen from the superposition of apo-*PaGT2* (light-brown) and ternary complex *PaGT2* (green). Phe309 and Phe312 from the opposite molecule of apo-*PaGT2*, occupying the ring structures of substrates, are also shown.

Crystal structure of *PaGT2* with substrates. To understand the catalytic mechanism in *PaGT2*, we obtained *PaGT2* crystals with donor analog UDP-2-fluoro-glucose (UDP-2FGlc) and stilbenoids, resveratrol, or pterostilbene (Figure 2b, Figure S3). We also performed crystallization of *PaGT2* with piceatannol and kaempferol; however, diffraction quality crystals were not obtained. The structure of *PaGT2* with UDP-2FGlc and resveratrol was refined to 2.60 Å resolution, and with pterostilbene to 2.65 Å resolution (Table S2). The a.u. of each ternary complex consists of three independent *PaGT2* molecules. The comparison of apo and ternary complex *PaGT2* structures shows that in the apo-*PaGT2*, the substrate-binding sites are occupied by the loop from opposite molecules in the a.u. It is seen that the sidechains of Phe309 and Phe312 from the opposite molecule mimicked the ring structures of the substrates. They are respectively placed at the position occupied by resorcinol/dimethylresorcinol (ring A) and 2-fluoro-glucose moieties of UDP-2FGlc (Figure 2C, 3A, 3B).

In the ternary complex of *PaGT2*, the C-terminal domain of each molecule shows a clear electron density for UDP-2FGlc which indicates the binding location of the sugar-donor (Figure S3). UDP-2FGlc is stabilized in *PaGT2* mainly by residues from the PSPG⁵⁸ motif that extends from Trp343 to Gln386 (Figure 3A, Figure S4). The uracil ring of UDP-2FGlc is placed between the sidechains of Trp343 and Gln346 and forms hydrogen bonds with the main chain nitrogen and oxygen atoms of Ala344. Gln346 and Glu369 form hydrogen bonds with the OH groups on the ribose moiety. The diphosphate is stabilized by interaction with His361, Asn365, and Ser366. The sidechain of Asn365 is observed to shift, making space to bind UDP-2FGlc. Tyr383, Gln386, Glu385, and Trp364 form hydrogen bonds and stabilize the 2-fluoro-glucose moiety. In the structure of *PaGT2*, some residues outside of the PSPG motif, Gly17, Thr137, Gln242, and Ser270, are also involved in the stabilization of the sugar-donor analog. The sugar-donor binding residues are shifted towards the sugar-donor analog, induced by the

binding of UDP-2FGlc. These sugar-donor binding residues are highly conserved among plant UGTs and their role in the recognition of UDP-sugar donor has been extensively studied elsewhere.^{57,20,32,35}

The aglycones bind to the N-terminal domains, similar to the binding of acceptors in other UGTs (Figure S3).^{20,23} The acceptor binding sites show the electron densities for resveratrol and pterostilbene in the respective ternary complexes. However, strong electron density maps are observed only for the resorcinol or resorcinol dimethyl ether moieties (ring A) of the acceptors. The electron density maps for the phenol moieties (ring B) are weaker in all *PaGT2* molecules. The sugar-acceptors are stabilized mainly through hydrophobic residues, Ile85, Leu116, Phe117, Phe136, Leu146, Val181, Pro183, Leu195, and Ala384 (Figure 3B). Polar residues, His18, His81, and Glu82, are present at the entrance, and Cys142 and Ser138 are placed at the interior of the active site. However, the distance between the polar residues of the enzyme and the OH or the OCH3 groups of the acceptors is large for strong interactions (Table S3). As suggested by the electron density maps, ring A of the substrates are oriented towards the interior of the acceptor binding pocket, while ring B is exposed to solvent. Ring A of the substrates is surrounded by more *PaGT2* residues and stabilized by stronger hydrophobic interactions compared to ring B. The poor stabilization of ring B of the substrates by *PaGT2* resulted in their weak electron density maps in the crystallographic data.

As seen in the crystal structures and from comparison with other UGT structures, His18 is recognized as the catalytic base in *PaGT2* which forms a catalytic dyad with Asp115. The catalytic histidine assists in the deprotonation of the hydroxyl group to form an acceptor nucleophile, which is considered as the main step in glycosylation by UGTs.^{31,21,35,20} In the crystal structures of *PaGT2*, the average distances from the putative glycosylation site (4'OH) on the stilbenoid acceptor to His18 is unexpectedly long (5.5 Å). Contrary, we found that another histidine residue (His81) is located 4.3

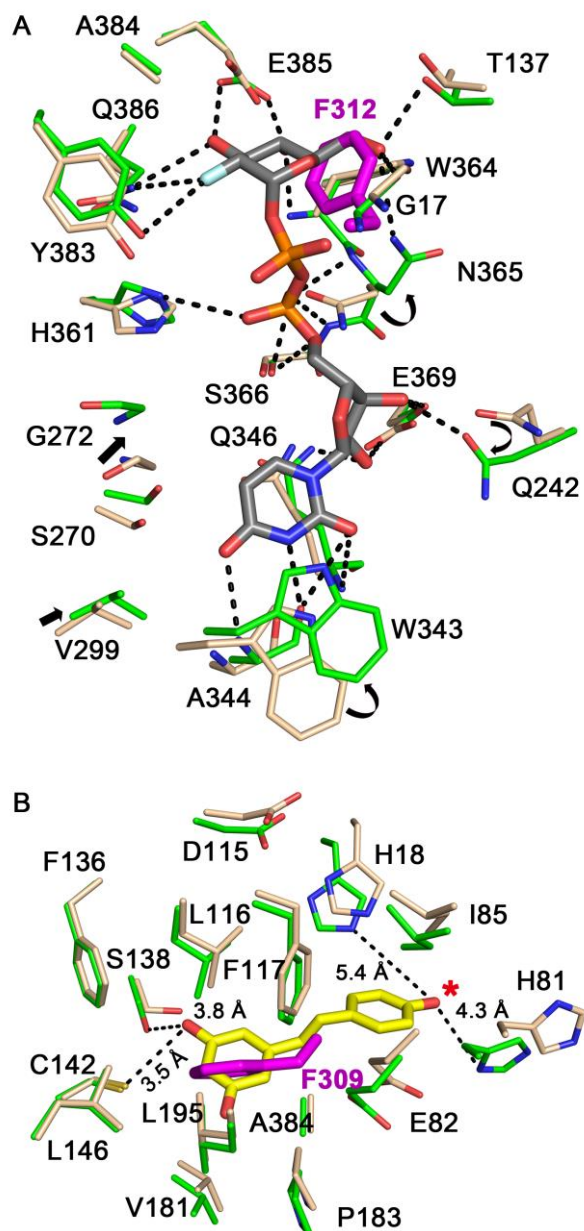


Figure 3: Substrates binding in *PaGT2*. (A) Residues involved in recognition of sugar donor are shown from both apo-*PaGT2* (light-brown) and ternary complex *PaGT2* (green). Donor analog in crystal structure UDP-2FGlc (grey) and Phe312 (magenta) from the opposite molecule in apo-crystal are shown. Hydrogen bonds are indicated with dotted lines. (B) Resveratrol in the acceptor binding site and residues of *PaGT2* from both apo (light-brown) and complex (green) structures. Distances between the polar sidechains and nearest hydroxyl group in resveratrol is indicated. The corresponding glycosylation site in piceatannol (4'OH) is indicated by *.

Å away from the 4'OH group. Although the distances between both histidines and the 4'OH groups on stilbenoids are long, His81 is closer to the 4'OH group than His18. This suggests that His81 in *PaGT2* can be involved in catalysis in addition to the conserved histidine (His18).

Molecular docking. Since the attempts to get the crystal structures of *PaGT2* with good acceptors piceatannol or kaempferol were not successful, we performed molecular docking of these compounds.

We also performed molecular docking of resveratrol and pterostilbene to confirm the accuracy of docking (Figure S5). Molecular docking of resveratrol and pterostilbene produced orientations of these substrates comparable to those in the crystal structures along with other possible orientations, which predicts the binding possibility of substrates in opposite orientations than observed in the crystal structures. The possibilities of binding of acceptors in the active-site other than those observed in the crystal structures have been predicted in UGT71G1 and V₁GT1.^{20,57} The crystal structures of UGT76G1 from *Stevia rebaudiana* have shown that its acceptor can bind in two opposite orientations in the active site.⁵⁹ The binding affinity of acceptors in the observed binding modes are comparable and are summarized in Table S4. Although, piceatannol and kaempferol can also bind to the active-site in different orientations (Figure S6), the formation of single glucoside products of each compound with high regioselectivity indicates that the binding orientations as shown in Figure 4 should be among the most suitable binding mode of these compounds in the wildtype *PaGT2*.

The molecular docking explains the specificity of *PaGT2* towards piceatannol and its low activity with other stilbenoids (Figure 4A). Although piceatannol has a similar backbone structure with resveratrol and pterostilbene, it contains an extra OH group at the 3' position. The 3'OH group on piceatannol is seen to interact with the sidechain of Glu82. The interaction of the 3'OH group on piceatannol and Glu82 plays an important role in its stabilization in the active site. Both resveratrol and pterostilbene lack such interaction with Glu82 due to the absence of a hydroxyl or polar group at the 3' position, which results in poor stabilization of these compounds. In the molecular docking of piceatannol, His81 is placed closer to the glycosylation site (the 4'OH of piceatannol) than the conserved catalytic histidine (His18), which is similar to the observations from the crystal structures. Thus, the piceatannol docking also indicates the possibility of both His18 and His81 as the catalytic residues in *PaGT2*.

In the molecular docking of kaempferol, His18 lies in the proximity to the 3OH group of kaempferol (Figure 4B). This is consistent with the glycosylation of kaempferol which exclusively forms kaempferol 3-*O*-β glucoside. The molecular docking of kaempferol also shows that, aside from Glu82, His81 is also involved in the stabilization of kaempferol. Glu82 and His81 interact with the O1 atom and the 4'OH group on kaempferol, respectively (Figure 4B). Similar to His81 or Glu82, polar residues at the entrance of the active site in V₁GT1 (Gln84)²⁰ and PtUGT1 (Glu88)⁵⁵ are reported to stabilize their respective substrates (Figure S7). Meanwhile, the main-chain carbonyl oxygen of Pro78 stabilizes the substrate in CtUGT78K6.²³ These earlier studies suggest that the residues located around the entrance of the acceptor binding site have an important role in the stabilization of substrates. Though it is inferred from the case of piceatannol that His81 could also be involved in catalysis to produce kaempferol 4'-*O*-β-glucoside, the analysis of kaempferol glucosylation product by NMR showed only the formation of kaempferol 3-*O*-β-glucoside, implying the non-catalytic role of His81 in kaempferol glucosylation by WT-*PaGT2*.

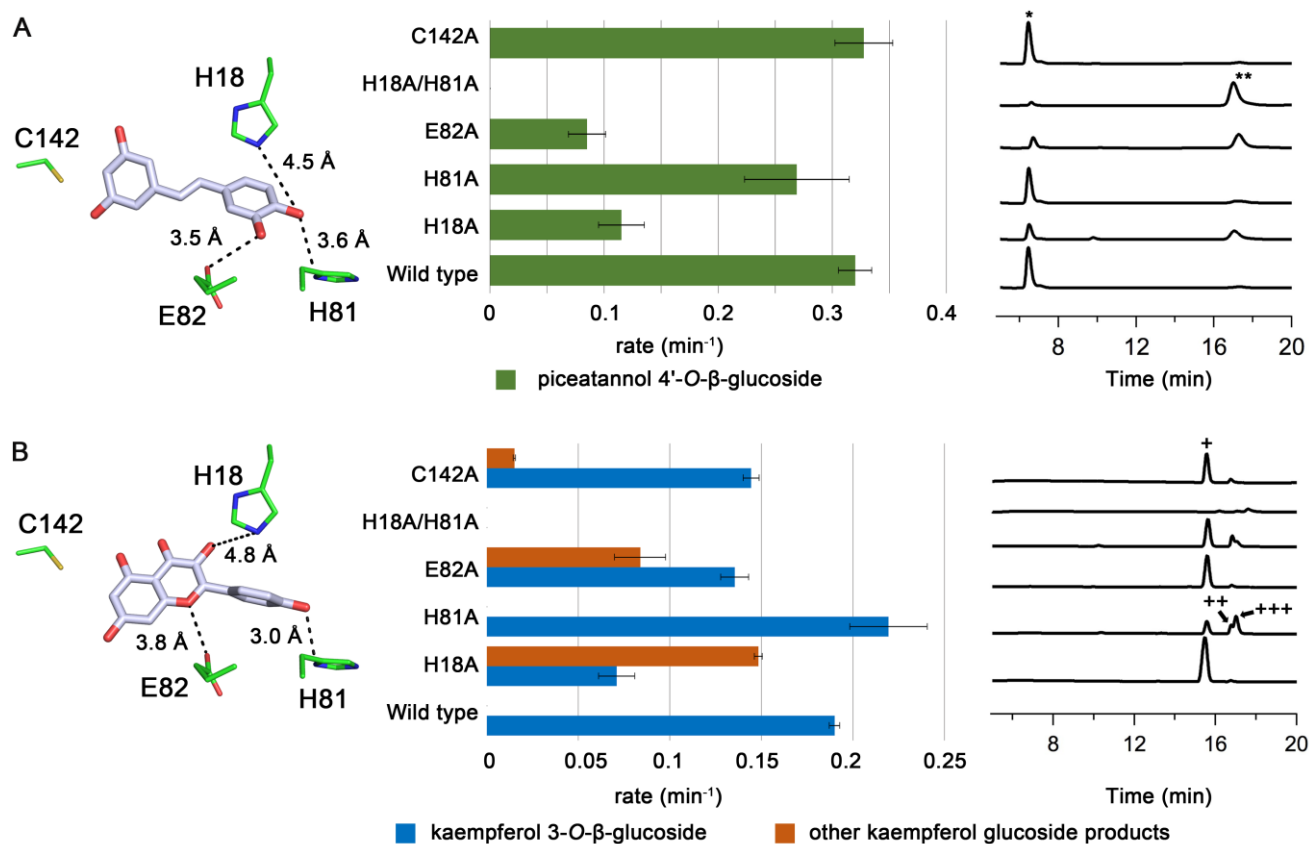


Figure 4: Molecular docking and Mutational assay. Polar residues in the acceptor binding site of *PaGT2* and (A) piceatannol and (B) kaempferol from the molecular docking. Right-side to each figure, the glycosylation activity of *PaGT2* mutants is presented in graph along with the HPLC chromatograms. (*piceatannol 4'-*O*- β -glucoside, **piceatannol, +kaempferol 3-*O*- β -glucoside, ++kaempferol 7-*O*- β -glucoside, and +++ other kaempferol glucoside. The peak for starting material kaempferol is not shown in the HPLC chromatograms (B), which is eluted by column washing.) The glycosylation was performed under standard reaction condition, the acceptor 50 μ M, UDP-glucose 100 μ M, enzyme 5 μ M at 37°C for 30min. The product concentration was divided by enzyme concentration 5 μ M and reaction time 30 min to calculate the average rate in 30 min.

Site-directed mutagenesis. For further exploration of the catalytic mechanism in *PaGT2*, we generated the site-directed mutants of the polar residues in the acceptor binding pocket and conducted enzyme assays. To determine the glycosylation ability of mutants, reaction mixtures containing 50 μ M acceptor, 100 μ M UDP-glucose, and 5 μ M mutant enzymes in 50 mM potassium phosphate buffer (pH 7.4) were incubated at 37 °C for 30 min. The reaction mixtures were analyzed by HPLC to determine the formation of products (Figure 4). The enzyme kinetic studies were conducted by varying the concentrations of acceptors. The list of mutants and their kinetic constants are listed in Table 1. Kinetic traces for piceatannol and kaempferol glycosylation by wildtype *PaGT2* and the mutants in the study are shown in Figure S8. A liner relationship between reaction time and product formation was observed in 20 min.

To clarify the role of His18 and His81 in catalysis, we substituted each histidine with alanine (Ala) and examined their glycosylation activity. The mutation of His81 to Ala results in an increase in the K_m values for both piceatannol and kaempferol by ~2 times. Besides, the catalytic efficiency (k_{cat}/K_m) of the His81Ala mutant is reduced. The mutant enzyme, which still maintains the activity, shows that the conserved histidine His18 function as the catalytic residue in *PaGT2*. Therefore, His81 is a key residue for substrate binding rather than a catalytic residue. The location of His81 at the opening of the acceptor-binding site and the flexibility of its

sidechain being exposed to solvent allows it to function as also a gate-keeper and prevent the escape of acceptors before glycosylation. The absence of His81 in the His81Ala mutant should have allowed the acceptors to easily escape from the active-site which is reflected with the increase in the K_m value. However, the His18Ala mutant can glycosylate piceatannol, although the catalytic efficiency (k_{cat}/K_m) dropped by 45%. Moreover, the catalytic efficiency of the His18Ala mutant for kaempferol glycosylation is unaffected, though the mutant enzyme loses the regioselectivity and forms a mixture of kaempferol glucosides including kaempferol 3-*O*- β glucoside. It is noteworthy that the substitution of His18 with Ala does not impair the catalytic activity of *PaGT2*, unlike that the mutation of the conserved histidine in many UGTs completely inactivates the enzyme.^{57,55,20,33} Therefore, we concluded that His18 is not an only catalytic residue and there should be the second catalytic residue in *PaGT2*. The reason the H18A mutant does not show regioselectivity for kaempferol is that the mutation at the active site with a shorter sidechain allows the binding of the acceptor in different conformations compared to that in the WT enzyme, which resulted in the formation of a mixture of kaempferol glucosides. Based on the obtained crystal structures and the mutational assay results, we hypothesize that His81 is another catalytic residue in *PaGT2*.

To further confirm the catalytic role of His81, we prepared a His18Ala/His81Ala double mutant and a mutant which lacked 31

N-terminal residues ($\Delta 31$) including the conserved catalytic histidine (His18). *PaGT2* is completely impaired by the introduction of His18Ala/His81Ala double mutation and does not form any detectable glucosides with both piceatannol and kaempferol (Figure 4). The possibility of Glu82, Ser138, and Cys142 in the active-site is ruled out by this result. Although these residues could be able to generate a nucleophile by abstracting a proton from the acceptor, the nucleophile would be too far from the C1 carbon atom on the glucose moiety of UDP-glucose, which could have prevented the formation of glucosylated products. In contrast, $\Delta 31$ retains the ability to glycosylate piceatannol, although its activity is highly diminished (Figure S9). The deletion of 31 N-terminal residues possibly distorted the enzyme's 3D structure and affected its glycosylation activity. The glycosylation ability of the $\Delta 31$ mutant shows that the mutant enzyme is still able to bind the substrates albeit lack of some secondary structures. Moreover, we also performed molecular docking of the acceptors with a *PaGT2* His18/81Ala mutant model-structure. The molecular docking results show the binding affinity of the compounds is comparable between the wildtype *PaGT2* and the His18/81Ala *PaGT2* (Table S4). Thus, we infer that the inactivation of His18/81Ala mutant enzyme is due to the lack of catalytic residue(s) and not due to the inability of the His18/81Ala mutant enzyme to bind the acceptors. These results confirm both His18 and His81 as catalytic residues in *PaGT2*. Furthermore, the ability to form glycoside products by both His18Ala and His81Ala mutants shows that both histidines can independently catalyze glycosylation. We propose that *PaGT2* can generate the acceptor nucleophile in two different ways as shown in scheme S1. Since both histidines in *PaGT2* can catalyze glycosylation, we called *PaGT2* as an ambidextrous glycosyltransferase.

The presence of an additional catalytic residue has been predicted in an isoflavonoid 7-*O*-glucosyltransferase *GmIF7GT* from *Glycyne max*³⁵. *GmIF7GT* lacking 49 N-terminal residues including the conserved catalytic histidine is reported to form glycoside products with the substrates. Furthermore, UGTs with non-conserved catalytic residue and without the catalytic dyad has been reported. For example, glycosylation in *CsUGT75L12*, a flavonoid 7-*O*-glycosyltransferase from *Camellia sinensis*, is catalyzed by Gln54 instead of the conserved histidine (His56)³⁶. Similarly, a single histidine catalyzes rhamnosylation in *UGT89C1* from *Arabidopsis thaliana*³², showing the His-Asp catalytic dyad is not always required for glycosylation in some UGTs. In *PaGT2* the conserved His-Asp catalytic pair could be important for catalysis in the wildtype enzyme and the His81Ala mutant. Conversely, in the His18Ala mutant, aspartate from the conserved His-Asp pair is less likely to have a role in the catalysis because this aspartate residue lies far and does not make direct contact with acceptors. Thus, the formation of glycosylated products by the His18Ala mutant supports these previous reports, where His81 is a non-conserved residue and does not require another residue to function as a catalytic pair. However, in contrast to these previous reports, *PaGT2* is the first UGT having two active catalytic residues at the same time and probably uses them separately depending on the cases.

We also performed the mutation of Glu82 that was determined to be important for the stabilization of acceptors in the active site. Mutation of Glu82 to Ala reduces the catalytic efficiency for piceatannol glycosylation by ~5 times compared to the wild type enzyme. The interaction between the 3'OH group and Glu82 is, therefore, necessary for piceatannol glycosylation as previously indicated by molecular docking. For overall kaempferol glycosylation, Glu82 does not seem to be important. However, the interaction between Glu82 and the O1 atom of kaempferol is necessary for regioselective kaempferol glycosylation. The Glu82Ala mutant is seen to

form a mixture of kaempferol glucosides including kaempferol 3-*O*- β -glucoside which is comparable to the formation of a mixture of kaempferol glucosides by His18Ala mutant. It should be noted that the His18Ala mutant and the Glu82Ala mutants lost the regioselectivity for kaempferol glucosylation but not in the case with the His81Ala mutant. His18 and Glu82 are located inside the active-site, whose replacement with Ala with shorter sidechain should have increased the volume. This could have increased the frequency of binding kaempferol in different orientations rather than the stable binding mode in the wildtype enzyme. Thus, in the His18Ala mutant different OH groups are placed closer to His81 in different binding modes and in the Glu82Ala mutant, in addition to the previous possibility, both histidine could have catalyzed glycosylation to form a mixture of kaempferol glucosides. Whereas, the size of the active-site is less affected by the mutation of His81 since it is placed at the opening of the acceptor binding pocket, which resulted in a single product comparable to the wildtype enzyme. The possible mechanism of nucleophile generation in kaempferol glycosylation is shown in scheme S2.

Structure-based modification of *PaGT2* for resveratrol glycosylation. Resveratrol, a stilbenoid polyphenol, has a broad range of biological activities and is a compound of interest for cosmetics, food and pharmaceutical industries.⁶⁰⁻⁶² While the low water solubility limits its uptake and complicates the development of therapeutics, the water-soluble glucoside derivatives of resveratrol are known to have similar effects as the parent compound.^{10,63} Resveratrol can primarily form two glucosides, namely resveratrol 3-*O*- β -glucoside and resveratrol 4'-*O*- β -glucoside. These glucosides show different pharmaco-kinetics and have advantages over each other.^{10,6} Hence, it is preferable to have an enzyme that produces the resveratrol glucosides with high regioselectivity.

Unfortunately, the poor stabilization of resveratrol in the active site results in the low activity of *PaGT2* towards it. Besides, it is seen in the crystal structure that none of the hydroxyl group on resveratrol is close enough to both catalytic histidine for effective interaction. It is well known that the mutation of amino acids in the active site can change the size of the active-site. Thus, the mutation of residues in the acceptor-binding pocket in *PaGT2* can change the position of resveratrol in the active-site and place one of the hydroxyl groups close to either of the catalytic histidines. In the crystal structure, it is seen that the sidechain of Cys142 protrudes into the active-site (Figure 5). The 3OH group of resveratrol is located at an average distance of 4.03 Å, which is suitable for the formation of a hydrogen bond between Cys142 and resveratrol (Table S3). However, this interaction between Cys142 and resveratrol could be one of the reasons that place resveratrol at an unsuitable distance,

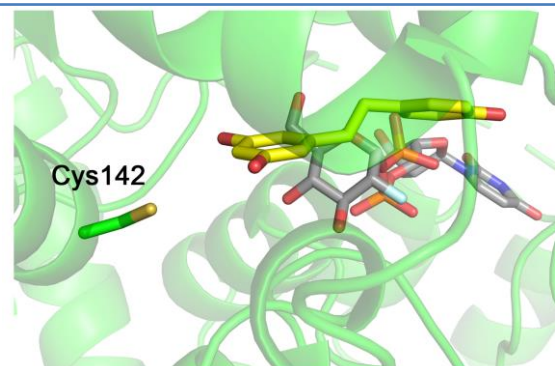


Figure 5: Position of Cys142 in the active-site. (A) Cys142 is placed at the rear side of acceptor binding pocket. Cys142 was mutated to other residues for changing the size of acceptor binding pocket.

as observed in the crystal structure, from either of the catalytic histidines in the active-site for glycosylation. We assumed that the mutation of Cys142 into amino-acids with varying sidechain length will alter the position of resveratrol in the active-site. Thus, we proceeded with the substitution of Cys142 with other amino acid residues. We replaced Cys142 with Ala, Phe, or Gln, which has different sidechain lengths. The mutation of Cys142 dramatically increased the glycosylation activity of *PaGT2* with resveratrol and endowed the enzyme with the ability to form resveratrol glucosides (Table 2). Among the three mutants, the Cys142Ala mutant had the highest activity with resveratrol and primarily formed resveratrol 3-*O*- β -glucoside with high regioselectivity. The Cys142Phe mutant also had high regioselectivity but formed resveratrol 4'-*O*- β -glucoside as a major product. The Cys142Gln mutant had the lowest activity with resveratrol as well as low regioselectivity and formed both resveratrol 3-*O*- β -glucoside and resveratrol 4'-*O*- β -glucoside at a nearly equal ratio. Possibly, these mutations allow resveratrol to bind in different positions and orientations compared to its binding in wild type *PaGT2*, such that one of the OH group on resveratrol is suitably placed close to either of the catalytic histidines for glycosylation.

Table 2. Resveratrol glycosylation activity of *PaGT2* Cys142 mutants

	Resveratrol 4' glucoside (turnover/min)	Resveratrol 3 glucoside (turnover/min)	Sum (turnover/min)
Wild type <i>PaGT2</i>	0	0	0
C142Q <i>PaGT2</i>	0.036 \pm 0.007	0.020 \pm 0.004	0.05 \pm 0.01
C142F <i>PaGT2</i>	0.072 \pm 0.014	0.007 \pm 0.001	0.08 \pm 0.014
C142A <i>PaGT2</i>	0.003 \pm 0.0004	0.307 \pm 0.036	0.31 \pm 0.041

We also evaluated the effect of the Cys142 mutations on piceatannol glycosylation (Table S5). The Cys142 mutations show a slight increase in the specific activity but do not affect regioselectivity for piceatannol glycosylation, meaning that we achieved engineering of *PaGT2* that regioselectively glucosylate both resveratrol and piceatannol. However, the regioselectivity of kaempferol glycosylation is affected by the Cys142Ala mutant. We infer that the mutation of Cys142 in *PaGT2* can be utilized to modulate the size of the active site which may be useful for changing the regioselectivity of glycosylation of acceptors.

CONCLUSION

We characterized a polyphenol glycosyltransferase, *PaGT2* from *P. americana*, by determining its crystal structures, performing molecular docking, and mutagenesis studies. The structures provide insights into the stilbenoid glycosylation mechanism. We recognized a non-conserved catalytic residue (His81) is present in addition to the conserved catalytic residue (His18) in *PaGT2* and show that both catalytic residues in *PaGT2* can independently catalyze glycosylation. Due to the ability of *PaGT2* to utilize both catalytic histidines independently for glycosylation, we called it as ambidextrous glycosyltransferase. Additionally, the structure-guided mutants of Cys142 endowed *PaGT2* with the ability to regioselectively glucosylate resveratrol. Cys142Ala and Cys142Phe mutants

formed resveratrol 3-*O*- β -glucoside and resveratrol 4'-*O*- β -glucoside, respectively with high regioselectivity. Thus, our results provide a basis for the modification of UGTs for efficient and regioselective glycosylation of compounds of interest.

ASSOCIATED CONTENT

Supporting Information

The Supporting Information is available free of charge on the ACS Publications website.

The PDB codes for apo-*PaGT2*, *PaGT2* with UDP-2F1c and resveratrol, and *PaGT2* with UDP-2FG1c and pterostilbene are 6JEL, 6JEM, and 6JEN, respectively.

AUTHOR INFORMATION

Corresponding Author

*hamada@dls.ous.ac.jp

*t_inoue@phs.osaka-u.ac.jp

*ozakis@yamaguchi-u.ac.jp

ORCID

Hiroki Hamada: <https://orcid.org/0000-0002-7877-3367>

Tsuyoshi Inoue: <https://orcid.org/0000-0001-5337-5066>

Shin-ichi Ozaki:

Author Contributions

R.M., Y.F., H.H., T.I., and S.O. designed research; R.M., N.S., and S.O. performed the assay and analyzed the results; K.K. and H.H. performed NMR analysis. Taisuke N. established protocols for protein purification and performed the preliminary crystallographic analysis; Toru N. contributed cloning of *PaGT2*; R.M. purified and crystallized proteins; R.M. and Y.F. collected and analyzed crystallographic data; R.M., Y.F., and S.O. wrote the paper with input from all authors.

Notes

The authors declare no competing financial interests.

ACKNOWLEDGMENT

The authors wish to thank Dr. K. Fujimoto, Fuji molecular planning co., Ltd. for the synthesis of UDP-2FG1c. The authors thank the beamline staff for their support during data collection on BL44XU at SPring-8 under proposal Nos. 2017A6745, 2017B6745, 2018A6844, and 2018B6844. This work was partly supported by Grant-in-Aid for Young Scientists (B) 17K17862 for YF, Grant-in-Aid for Scientific Research (B) 18H02004 for TI, and Grant-in-Aid for Scientific Research (C) 17K05933 for SO.

REFERENCES

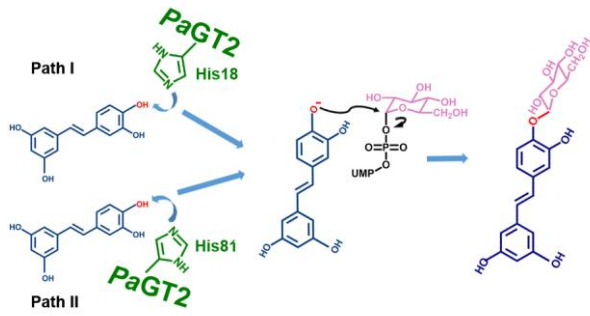
- Lairson, L. L., Henrissat, B., Davies, G. J., and Withers, S. G. (2008) Glycosyltransferases: structures, functions, and mechanisms, *Annual review of biochemistry* 77, 521–555.
- Bowles, D., Isayenkova, J., Lim, E. K., and Poppenberger, B. (2005) Glycosyltransferases: managers of small molecules, *Current opinion in plant biology* 8, 254–263.

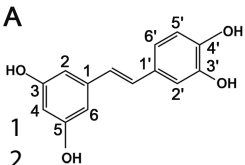
3. Härtl, K., Huang, F.-C., Giri, A. P., Franz-Oberdorf, K., Frotscher, J., Shao, Y., Hoffmann, T., and Schwab, W. (2017) Glucosylation of Smoke-Derived Volatiles in Grapevine (*Vitis vinifera*) is Catalyzed by a Promiscuous Resveratrol/Guaiacol Glucosyltransferase, *Journal of agricultural and food chemistry* 65, 5681–5689.
4. Yoshimura, M., Amakura, Y., Tokuhara, M., and Yoshida, T. (2008) Polyphenolic compounds isolated from the leaves of *Myrtus communis*, *Journal of natural medicines* 62, 366–368.
5. Rahman, M. A. A., and Moon Surk-Sik (2007) Antioxidant Polyphenol Glycosides from the Plant *Draba nemorosa*, *Bulletin of the Korean Chemical Society* 28, 827–831.
6. Lepak, A., Gutmann, A., Kulmer, S. T., and Nidetzky, B. (2015) Creating a Water-Soluble Resveratrol-Based Antioxidant by Site-Selective Enzymatic Glucosylation, *Chembiochem : a European journal of chemical biology* 16, 1870–1874.
7. Akinwumi, B. C., Bordun, K.-A. M., and Anderson, H. D. (2018) Biological Activities of Stilbenoids, *International journal of molecular sciences* 19.
8. Ross, J. A., and Kasum, C. M. (2002) Dietary flavonoids: bioavailability, metabolic effects, and safety, *Annual review of nutrition* 22, 19–34.
9. Quideau, S., Deffieux, D., Douat-Casassus, C., and Pouységue, L. (2011) Plant polyphenols: chemical properties, biological activities, and synthesis, *Angewandte Chemie (International ed. in English)* 50, 586–621.
10. Hosoda, R., Kuno, A., Hori, Y. S., Ohtani, K., Wakamiya, N., Oohiro, A., Hamada, H., and Horio, Y. (2013) Differential cell-protective function of two resveratrol (trans-3,5,4'-trihydroxystilbene) glucosides against oxidative stress, *The Journal of pharmacology and experimental therapeutics* 344, 124–132.
11. Dai, L., Li, J., Yao, P., Zhu, Y., Men, Y., Zeng, Y., Yang, J., and Sun, Y. (2017) Exploiting the aglycon promiscuity of glucosyltransferase Bs-YjiC from *Bacillus subtilis* and its application in synthesis of glycosides, *Journal of biotechnology* 248, 69–76.
12. Lim, E.-K. (2005) Plant glucosyltransferases: their potential as novel biocatalysts, *Chemistry (Weinheim an der Bergstrasse, Germany)* 11, 5486–5494.
13. Lombard, V., Golaconda Ramulu, H., Drula, E., Coutinho, P. M., and Henrissat, B. (2014) The carbohydrate-active enzymes database (CAZy) in 2013, *Nucleic acids research* 42, D490–D495.
14. Wen, C., Huang, W., Zhu, X. L., Li, X. S., Zhang, F., and Jiang, R. W. (2018) UGT74AN1, a Permissive Glycosyltransferase from *Asclepias curassavica* for the Regiospecific Steroid 3-O-Glycosylation, *Organic letters* 20, 534–537.
15. Noguchi, A., Kunikane, S., Homma, H., Liu, W., Sekiya, T., Hosoya, M., Kwon, S., Ohiwa, S., Katsuragi, H., Nishino, T., Takahashi, S., Hamada, H., and Nakayama, T. (2009) Identification of an inducible glucosyltransferase from *Phytolacca americana* L. cells that are capable of glucosylating capsaicin, *Plant Biotechnology* 26, 285–292.
16. Noguchi, A., Horikawa, M., Fukui, Y., Fukuchi-Mizutani, M., Iuchi-Okada, A., Ishiguro, M., Kiso, Y., Nakayama, T., and Ono, E. (2009) Local differentiation of sugar donor specificity of flavonoid glucosyltransferase in *Lamiales*, *The Plant cell* 21, 1556–1572.
17. Gurung, R. B., Kim, E.-H., Oh, T.-J., and Sohng, J. K. (2013) Enzymatic synthesis of apigenin glucosides by glucosyltransferase (YjiC) from *Bacillus licheniformis* DSM 13, *Molecules and cells* 36, 355–361.
18. Pandey, R. P., Parajuli, P., Koirala, N., Park, J. W., and Sohng, J. K. (2013) Probing 3-hydroxyflavone for in vitro glycorandomization of flavonols by YjiC, *Applied and environmental microbiology* 79, 6833–6838.
19. Zhou, M., and Thorson, J. S. (2011) Asymmetric enzymatic glycosylation of mitoxantrone, *Organic letters* 13, 2786–2788.
20. Offen, W., Martinez, C. F., Yang, M., Lim, E. K., Davis, B. G., Tarling, C. A., Ford, C. M., Bowles, D. J., and Davies, G. J. (2006) Structure of a flavonoid glucosyltransferase reveals the basis for plant natural product modification, *EMBO J.* 25, 1396–1405.
21. Li, L., Modolo, L. V., Escamilla-Trevino, L. L., Achnine, L., Dixon, R. A., and Wang, X. (2007) Crystal structure of *Medicago truncatula* UGT85H2—insights into the structural basis of a multifunctional (iso)flavonoid glucosyltransferase, *Journal of Molecular Biology* 370, 951–963.
22. He, X.-Z., Wang, X., and Dixon, R. A. (2006) Mutational analysis of the *Medicago* glucosyltransferase UGT71G1 reveals residues that control regioselectivity for (iso)flavonoid glycosylation, *The Journal of biological chemistry* 281, 34441–34447.
23. Hiromoto, T., Honjo, E., Noda, N., Tamada, T., Kazuma, K., Suzuki, M., Blaber, M., and Kuroki, R. (2015) Structural basis for acceptor-substrate recognition of UDP-glucose: anthocyanidin 3-O-glucosyltransferase from *Clitoria ternatea*, *Protein science : a publication of the Protein Society* 24, 395–407.
24. Bolam, D. N., Roberts, S., Proctor, M. R., Turkenburg, J. P., Dodson, E. J., Martinez-Fleites, C., Yang, M., Davis, B. G., Davies, G. J., and Gilbert, H. J. (2007) The crystal structure of two macrolide glucosyltransferases provides a blueprint for host cell antibiotic immunity, *Proceedings of the National Academy of Sciences of the United States of America* 104, 5336–5341.
25. Gantt, R. W., Peltier-Pain, P., Singh, S., Zhou, M., and Thorson, J. S. (2013) Broadening the scope of glucosyltransferase-catalyzed sugar nucleotide synthesis, *Proceedings of the National Academy of Sciences of the United States of America* 110, 7648–7653.
26. Gantt, R. W., Goff, R. D., Williams, G. J., and Thorson, J. S. (2008) Probing the aglycon promiscuity of an engineered glucosyltransferase, *Angewandte Chemie (International ed. in English)* 47, 8889–8892.
27. Ma, W., Zhao, L., Ma, Y., Li, Y., Qin, S., and He, B. (2020) Oriented efficient biosynthesis of rare ginsenoside Rh2 from PPD by compiling UGT-YjiC mutant with sucrose synthase, *International journal of biological macromolecules* 146, 853–859.
28. Williams, G. J., Zhang, C., and Thorson, J. S. (2007) Expanding the promiscuity of a natural-product glucosyltransferase by directed evolution, *Nature chemical biology* 3, 657–662.
29. Kim, T.-S., Le, T. T., Nguyen, H. T., Cho, K. W., and Sohng, J. K. (2018) Mutational analyses for product specificity of YjiC towards α -mangostin mono-glucoside, *Enzyme and microbial technology* 118, 76–82.

30. Lim, E. K., and Bowles, D. J. (2004) A class of plant glycosyltransferases involved in cellular homeostasis, *The EMBO journal* 23, 2915–2922.
31. Brazier-Hicks, M., Offen, W. A., Gershtater, M. C., Revett, T. J., Lim, E.-K., Bowles, D. J., Davies, G. J., and Edwards, R. (2007) Characterization and engineering of the bifunctional N- and O-glucosyltransferase involved in xenobiotic metabolism in plants, *Proceedings of the National Academy of Sciences of the United States of America* 104, 20238–20243.
32. Zong, G., Fei, S., Liu, X., Li, J., Gao, Y., Yang, X., Wang, X., and Shen, Y. (2019) Crystal structures of rhamnosyltransferase UGT89C1 from *Arabidopsis thaliana* reveal the molecular basis of sugar donor specificity for UDP- β -l-rhamnose and rhamnosylation mechanism, *The Plant journal : for cell and molecular biology* 99, 257–269.
33. Ozaki, S.-i., Imai, H., Iwakiri, T., Sato, T., Shimoda, K., Nakayama, T., and Hamada, H. (2012) Regioselective glucosidation of trans-resveratrol in *Escherichia coli* expressing glucosyltransferase from *Phytolacca americana*, *Biotechnology letters* 34, 475–481.
34. Wang, X. (2009) Structure, mechanism and engineering of plant natural product glycosyltransferases, *FEBS letters* 583, 3303–3309.
35. Noguchi, A., Saito, A., Homma, Y., Nakao, M., Sasaki, N., Nishino, T., Takahashi, S., and Nakayama, T. (2007) A UDP-glucose:isoflavone 7-O-glucosyltransferase from the roots of soybean (*Glycine max*) seedlings. Purification, gene cloning, phylogenetics, and an implication for an alternative strategy of enzyme catalysis, *The Journal of biological chemistry* 282, 23581–23590.
36. Dai, X., Zhuang, J., Wu, Y., Wang, P., Zhao, G., Liu, Y., Jiang, X., Gao, L., and Xia, T. (2017) Identification of a Flavonoid Glucosyltransferase Involved in 7-OH Site Glycosylation in Tea plants (*Camellia sinensis*), *Scientific reports* 7, 5926.
37. Wang, L., Bai, L., Nagasawa, T., Hasegawa, T., Yang, X., Sakai, J.-i., Bai, Y., Kataoka, T., Oka, S., Hirose, K., Tomida, A., Tsuruo, T., and Ando, M. (2008) Bioactive triterpene saponins from the roots of *Phytolacca americana*, *Journal of natural products* 71, 35–40.
38. Iwakiri, T., Mase, S., Murakami, T., Matsumoto, M., Hamada, H., Nakayama, T., and Ozaki, S.-i. (2013) Glucosylation of hydroxyflavones by glucosyltransferases from *Phytolacca americana*, *Journal of Molecular Catalysis B: Enzymatic* 90, 61–65.
39. Hamada, H., Shimoda, K., Shimizu, N., Shimizu, Y., and Akagi, M. (2014) Synthesis of Glycosides of Resveratrol, Pterostilbene, and Piceatannol by Glucosyltransferase from *Phytolacca americana* Expressed in *Bacillus subtilis* and their Chemopreventive Activity Against Cancer, Allergic, and Alzheimer's Diseases, *Glycobiology Insights* 4, 1–6.
40. Yim, S. H., Lee, Y. J., Park, K. D., Lee, I. S., Shin, B. A., Jung, D. W., Williams, D. R., and Kim, H. J. (2015) Phenolic Constituents from the Flowers of *Hamamelis japonica* Sieb. et Zucc, *Nat Prod Sci* 21, 162–169.
41. Rhayem, Y., Théron, P., Camont, L., Couturier, M., Beaudeau, J.-L., Legrand, A., Jore, D., Gardés-Albert, M., and Bonnefont-Rousselot, D. (2008) Chain-breaking activity of resveratrol and piceatannol in a linoleate micellar model, *Chemistry and physics of lipids* 155, 48–56.
42. R. Telange, D., T. Patil, A., Tatode, A., and Bhojar, B. (2014) Development and Validation of UV Spectrophotometric Method for the Estimation of Kaempferol in Kaempferol: Hydrogenated Soy PhosphatidylCholine (HSPC) Complex, *Phm* 5, 34–38.
43. Otwinowski, Z., and Minor, W. (1997) 20 Processing of X-ray diffraction data collected in oscillation mode, *Methods in enzymology* 276, 307–326.
44. Kabsch, W. (2010) XDS, *Acta crystallographica. Section D, Biological crystallography* 66, 125–132.
45. Vagin, A., and Teplyakov, A. (2010) Molecular replacement with MOLREP, *Acta crystallographica. Section D, Biological crystallography* 66, 22–25.
46. Winn, M. D., Ballard, C. C., Cowtan, K. D., Dodson, E. J., Emsley, P., Evans, P. R., Keegan, R. M., Krissinel, E. B., Leslie, A. G. W., McCoy, A., McNicholas, S. J., Murshudov, G. N., Pannu, N. S., Potterton, E. A., Powell, H. R., Read, R. J., Vagin, A., and Wilson, K. S. (2011) Overview of the CCP4 suite and current developments, *Acta crystallographica. Section D, Biological crystallography* 67, 235–242.
47. Emsley, P., Lohkamp, B., Scott, W. G., and Cowtan, K. (2010) Features and development of Coot, *Acta crystallographica. Section D, Biological crystallography* 66, 486–501.
48. Kovalevskiy, O., Nicholls, R. A., Long, F., Carlon, A., and Murshudov, G. N. (2018) Overview of refinement procedures within REFMAC5: utilizing data from different sources, *Acta crystallographica. Section D, Structural biology* 74, 215–227.
49. Schrödinger, L. L.C. (2015) The PyMOL Molecular Graphics System, Version 1.8.
50. Wallace, A. C., Laskowski, R. A., and Thornton, J. M. (1995) LIGPLOT: a program to generate schematic diagrams of protein-ligand interactions, *Protein engineering* 8, 127–134.
51. Dallakyan, S., and Olson, A. J. (2015) Small-molecule library screening by docking with PyRx, *Methods in molecular biology (Clifton, N.J.)* 1263, 243–250.
52. Trott, O., and Olson, A. J. (2010) AutoDock Vina: improving the speed and accuracy of docking with a new scoring function, efficient optimization, and multithreading, *Journal of computational chemistry* 31, 455–461.
53. Gibson, R. P., Tarling, C. A., Roberts, S., Withers, S. G., and Davies, G. J. (2004) The donor subsite of trehalose-6-phosphate synthase: binary complexes with UDP-glucose and UDP-2-deoxy-2-fluoro-glucose at 2 Å resolution, *The Journal of biological chemistry* 279, 1950–1955.
54. Holm, L. (2019) Benchmarking Fold Detection by DaliLite v.5, *Bioinformatics* 35, 5326–5327.
55. Hsu, T. M., Welner, D. H., Russ, Z. N., Cervantes, B., Prathuri, R. L., Adams, P. D., and Dueber, J. E. (2018) Employing a biochemical protecting group for a sustainable indigo dyeing strategy, *Nature chemical biology* 14, 256–261.
56. He, J. B., Zhao, P., Hu, Z. M., Liu, S., Kuang, Y., Zhang, M., Li, B., Yun, C. H., Qiao, X., and Ye, M. (2019) Molecular and Structural Characterization of a Promiscuous C -Glycosyltransferase from *Trollius chinensis*, *Angew. Chem.* 58, 11513–11520.

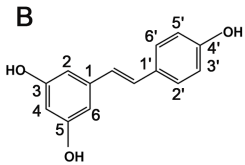
- 1
2
3
4
5
6
7
8
9
10
11
12
13
14
15
16
17
18
19
20
21
22
23
24
25
26
27
28
29
30
31
32
33
34
35
36
37
38
39
40
41
42
43
44
45
46
47
48
49
50
51
52
53
54
55
56
57
58
59
60
57. Shao, H., He, X., Achnine, L., Blount, J. W., Dixon, R. A., and Wang, X. (2005) Crystal structures of a multifunctional triterpene/flavonoid glycosyltransferase from *Medicago truncatula*, *The Plant cell* 17, 3141–3154.
58. Lim, E.-K., and Bowles, D. J. (2004) A class of plant glycosyltransferases involved in cellular homeostasis, *The EMBO journal* 23, 2915–2922.
59. Yang, T., Zhang, J., Ke, D., Yang, W., Tang, M., Jiang, J., Cheng, G., Li, J., Cheng, W., Wei, Y., Li, Q., Naismith, J. H., and Zhu, X. (2019) Hydrophobic recognition allows the glycosyltransferase UGT76G1 to catalyze its substrate in two orientations, *Nature communications* 10, 3214.
60. Dirks-Hofmeister, M. E., Verhaeghe, T., De Winter, K., and Desmet, T. (2015) Creating Space for Large Acceptors: Rational Biocatalyst Design for Resveratrol Glycosylation in an Aqueous System, *Angew. Chem.* 127, 9421–9424.
61. Ligt, M. de, Timmers, S., and Schrauwen, P. (2015) Resveratrol and obesity: Can resveratrol relieve metabolic disturbances?, *Biochimica et biophysica acta* 1852, 1137–1144.
62. Stivala, L. A., Savio, M., Carafoli, F., Perucca, P., Bianchi, L., Maga, G., Forti, L., Pagnoni, U. M., Albin, A., Prosperi, E., and Vannini, V. (2001) Specific structural determinants are responsible for the antioxidant activity and the cell cycle effects of resveratrol, *The Journal of biological chemistry* 276, 22586–22594.
63. Shimoda, K., Kubota, N., Uesugi, D., Hamada, H., Tanigawa, M., and Hamada, H. (2015) Synthesis and pharmacological evaluation of glycosides of resveratrol, pterostilbene, and piceatannol, *Annals of the New York Academy of Sciences* 1348, 141–149.

Insert Table of Contents artwork here

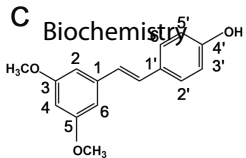




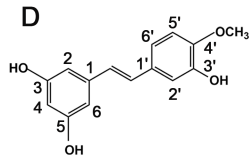
Piceatannol



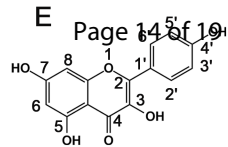
Resveratrol



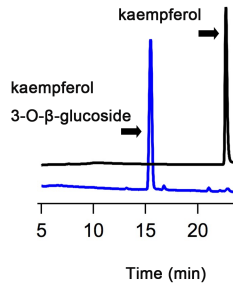
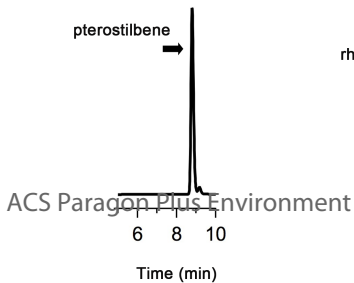
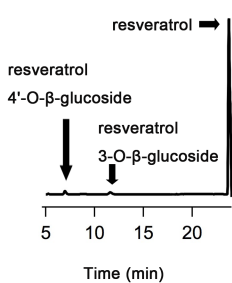
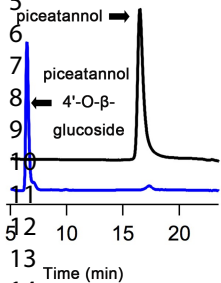
Pterostilbene



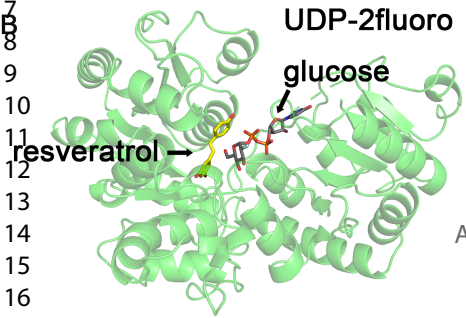
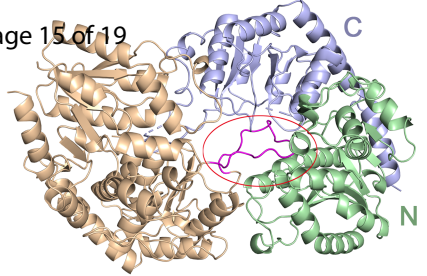
Rhapontigenin



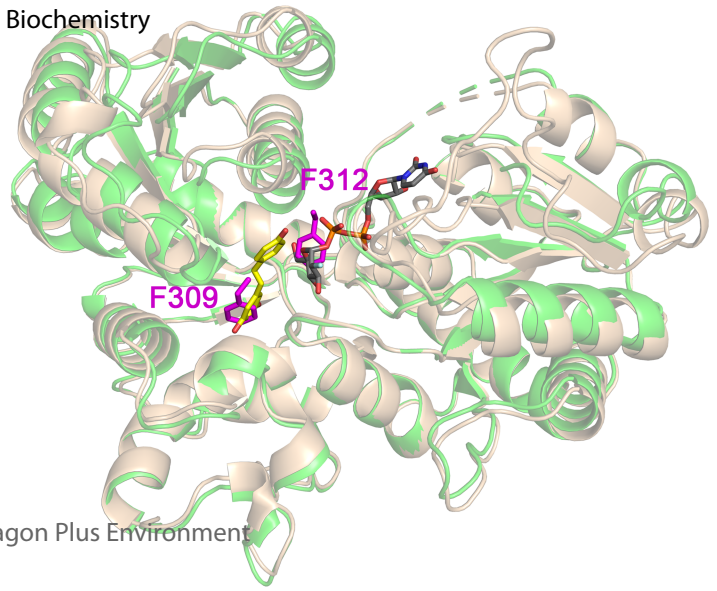
Kaempferol

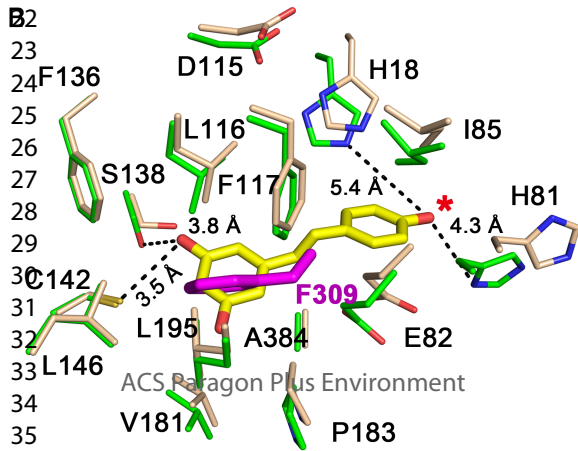
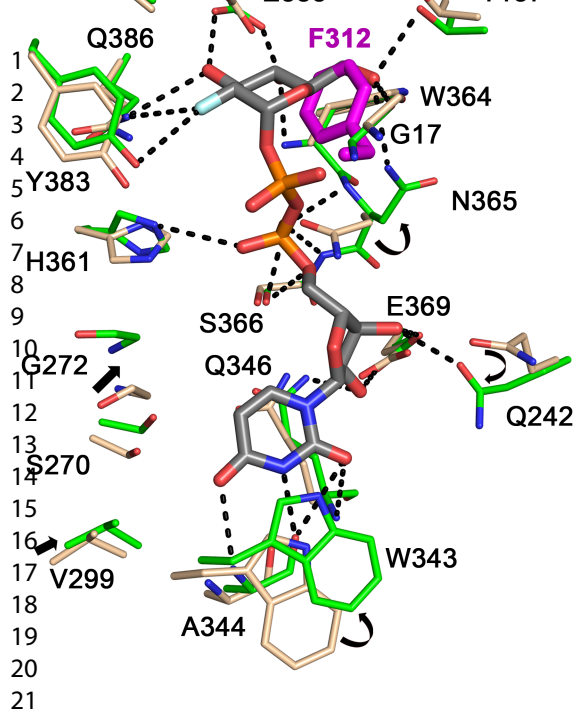


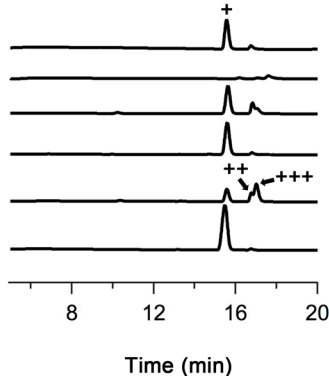
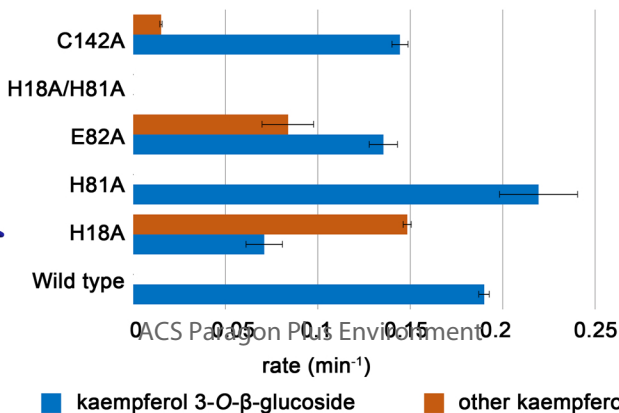
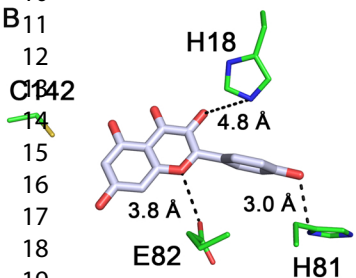
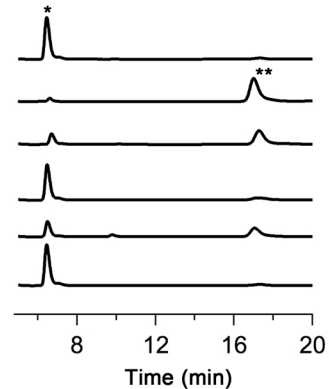
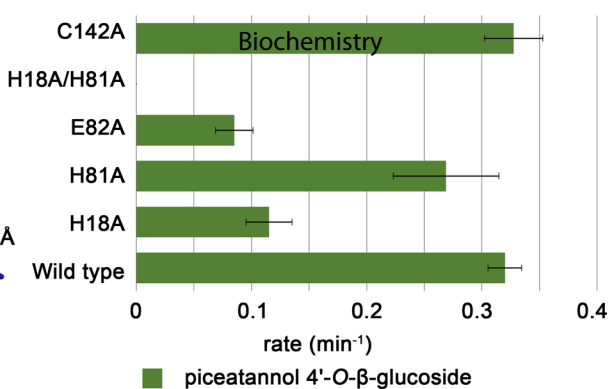
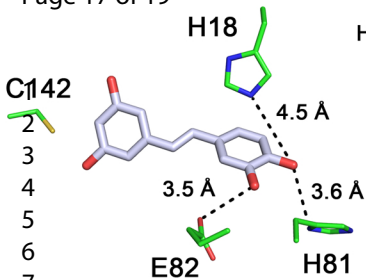
1
2
3
4
5
6
7
8
9
10
11
12
13
14
15
16
17



C Biochemistry

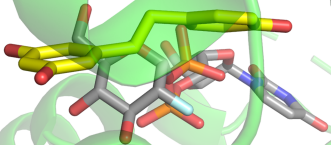
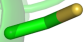






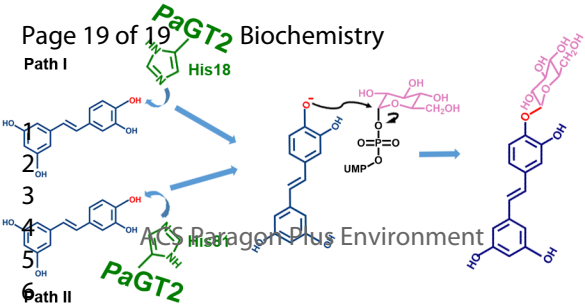
1
2
3
4
5
6
7
8

Cys142



ACS Paragon Plus Environment

Path I



ACS Paragon Plus Environment

Path II

7